

# Ballistic transport and electrostatics in metallic carbon nanotubes

A. Svizhenko\*, M. P. Anantram<sup>†</sup> and T. R. Govindan<sup>‡</sup>

Center for Nanotechnology and NASA Advanced Supercomputing Division,

NASA Ames Research Center,

Mail Stop: \*229-1 <sup>†</sup>229-1 <sup>‡</sup>258-5

Moffett Field, CA 94035-1000

Email: \*svizhenk@nas.nasa.gov <sup>†</sup>anant@mail.arc.nasa.gov <sup>‡</sup>Tr.R.Govindan@nasa.gov

**Abstract**—We calculate the current and electrostatic potential drop in metallic carbon nanotube wires self-consistently, by solving the Green's function and electrostatics equations in the ballistic case. About one tenth of the applied voltage drops across the bulk of a nanowire, independent of the lengths considered here. The remaining nine tenths of the bias drops near the contacts, thereby creating a non linear potential drop. The scaling of the electric field at the center of the nanotube with length ( $L$ ) is faster than  $1/L$  (roughly  $1/L^{1.25-1.75}$ ). At room temperature, the low bias conductance of large diameter nanotubes is larger than  $4e^2/h$  due to occupation of non crossing subbands. The physics of conductance evolution with bias due to the transmission Zener tunneling in non crossing subbands is discussed.

**Index Terms**—Nanowires, carbon nanotubes, interconnects, ballistic transport, modeling.

## I. INTRODUCTION

Carbon nanotubes have the potential to make good interconnects because current densities approaching  $10^9$  A/cm<sup>2</sup> [1] and compatibility with silicon technology [2], [3] have been demonstrated. In the use of multiwall nanotubes for such applications, contact with as many layers of the tube as possible [4] is desirable. Larger diameter nanotubes are preferable because even the semiconducting shells can carry current due to small bandgaps. For example, a semiconducting shell with a radius of 18.8 nm has a half bandgap of only 62.5 meV ( $kT=26$  meV at room temperature). Experimentally measured conductance of metallic carbon nanotubes is close to the theoretical maximum of  $4e^2/h$  at low biases [5], [6], [7], [8].

Experiments on small diameter carbon nanotubes show that the differential conductance decreases with applied bias, for voltages larger than 100 - 200 meV [9], [10], [11]. Ref. [9] found that the conductance decrease with increase in bias was caused by reflection of incident electrons at crossing subbands due to scattering with zone boundary phonons. Measured values of the mean free path [12] are in the range of 0.1 - 1  $\mu$ m at low bias and around 10 nm at high bias for 1.8 nm diameter nanotubes (corresponds to a (24,0) nanotube). Simple estimates of scattering rates [12], [13] show inverse dependence with nanotube diameter, which suggests that phonon scattering is less important in large diameter nanotubes.

The non crossing subbands of small diameter nanotubes do not carry current due to their large band gap. In contrast, large diameter nanotubes experimentally show an increase in conductance with applied bias [5], [6], [14], [15]. Reference [16] suggested that as the diameter increases electrons may tunnel into non crossing subbands, thus causing an increase in differential conductance with applied bias. The main drawbacks of the calculation in reference [16] was that the results depended on the assumed form of potential drop in metallic nanotubes (charge self-consistency and phonon scattering were neglected).

Apart from measuring current-voltage characteristics, the potential drop can be measured by EFM. Refs. [17] found that the potential drop in a single wall nanotube was small compared to a multiwall nanotube.

In this work, we computationally model ballistic electron flow in metallic nanowires within a tight-binding approximation by including *charge self consistency*, which is an important factor in determining the current. The potential distribution and current-voltage characteristics are studied as a function of both nanotube diameter and length. In 3D (bulk) crystal the electric field, potential and net charge at the edges of the tube would decay exponentially, resulting in zero net charge and zero electric field inside the conductor. In a 1D wire, even perfectly ballistic, the screening is poorer, due to the lower electron density of states. Reference [18] found that near  $p$ - $n$  junctions in semiconducting nanotubes, this leads to a very long range ( $\sim 1/\ln(y)$ ) tail in the charge distribution and, consequently, a non zero electric field very far from the junction. It is however an open question whether metallic nanotubes also have poor screening properties. Here we use an electrostatics model similar to that in [18], but significantly improve on transport, using Non Equilibrium Green's Function formalism. The ballistic approximation works well at low bias and/or in large diameter nanotubes. The detailed study of phonon scattering effects will be given elsewhere.

The nature of the metallic contacts is also important. From an experimental view point the contact between a metal and a nanotube can either be an end-contact or side-contact. The end-contact corresponds to only the nanotube

tip making the contact to the metal lead. In experiments, the end-contacts usually include strong chemical modification of the nanotube at the metal-nanotube interface. Also, reference [5] found that end-contacts without sufficient chemical modification of the nanotube-metal interface have a large contact resistance. In such configuration, electrons are injected directly from the metal to the nanotube region between the contacts. Due to the uncertainty of the contact bandstructure, modeling end-contacts even remotely correct is extremely difficult.

The side-contacts correspond to coupling between metal and nanotube atoms over many unit cells of the nanotube, and can be thought of as a nanotube buried inside a metal. Most experimental configurations correspond to side-contacts [5], [19]. An important feature of the side contacts is that the coupling between atoms in the nanotube is much stronger than coupling between nanotube and metal atoms which means that the bandstructure of the contacts can be assumed to be the same as that of the nanotube between the contacts. In the side-contact geometry, electrons are predominantly injected from the metal into the nanotube buried in the metal and then transmitted to the nanotube region between the contacts. In fact, as proof of such a process, scaling of conductance with contact area has been observed in the side-contacted geometry by references [5], [19]. Modeling showed that the conductance in metallic zigzag nanotubes can be close to the theoretical maximum for conductance with sufficient overlap area in the contact [20].

In the work presented here, we assume "perfect" contacts to represent an ideal side-contacted nanotube. The details of the contact model will be given below.

## II. FORMALISM

In this paper we consider only zigzag carbon nanotubes. The analysis for armchair nanotubes is similar. The general form of the Hamiltonian for electrons in a carbon nanotube can be written as:

$$H = \sum_{i,x} U_x^i c_{i,x}^\dagger c_{i,x} + \sum_{i,j,x,x'} t_{x,x'}^{i,j} c_{i,x}^\dagger c_{j,x'} \quad (1)$$

The sum is taken over all rings  $i, j$  in transport direction and all atoms located at  $x, x'$  in each ring. We make the following common approximations: i) only nearest neighbors are included; each atom in an  $sp^2$ -coordinated carbon nanotube has three nearest neighbors, located  $a_{cc} = 1.42 \text{ \AA}$  away; ii) the bandstructure consists of only  $\pi$ -orbital, with the hopping parameter  $t_o = V_{pp\pi} = -2.77 \text{ eV}$  and the on-site potential  $U_o = \epsilon_p = 0$ . Such a tight-binding model is adequate to model transport properties in undeformed nanotubes. Within these approximations, only

the following parameters are non zero:

$$\begin{aligned} U_x^i &= U_o, \forall i \\ t_{x,x'}^{i,i-1} &= t_{x,x'}^{i-1,i} = t_o \delta_{x \pm a/2, x'}, \forall i = 2k \\ t_{x,x'}^{i,i+1} &= t_{x,x'}^{i+1,i} = t_o \delta_{x, x'}, \forall i = 2k, \end{aligned} \quad (2)$$

where  $a = a_{cc}\sqrt{3}$ . In  $(N, 0)$  zigzag nanotubes, the wave vector in the circumferential direction is quantized as  $\tilde{q} = 2\pi q/Na$ ,  $q = 1, 2, \dots, N$ , creating eigenmodes in the energy spectrum. By doing a Fourier expansion of  $c_{i,x}^\dagger$  and  $c_{i,x}$  in  $\tilde{q}$ -space and using (2) we obtain a decoupled electron Hamiltonian in the eigenmode space:

$$H = \sum_q H^q \quad (3)$$

$$H^q = \sum_i (U_{\tilde{q}}^i c_{i,\tilde{q}}^\dagger c_{i,\tilde{q}} + t_{\tilde{q}}^{i,i\pm 1} c_{i,\tilde{q}}^\dagger c_{i\pm 1,\tilde{q}}) \quad (4)$$

where

$$\begin{aligned} U_{\tilde{q}}^i &= U_o, \forall i \\ t_{\tilde{q}}^{i,i-1} &= t_{\tilde{q}}^{i-1,i} = 2t_o \cos\left(\frac{\tilde{q}a}{2}\right) \equiv t_1, \forall i = 2k \\ t_{\tilde{q}}^{i,i+1} &= t_{\tilde{q}}^{i+1,i} = t_o \equiv t_2, \forall i = 2k \end{aligned} \quad (5)$$

The 1-D tight-binding Hamiltonian  $H^q$  describes a chain with two sites per unit cell with on-site potential  $U_o$  and hopping parameters  $t_1$  and  $t_2$  (Fig. 1). For numerical solution, the spatial grid corresponds to the rings of the nanotube, separated by  $a/2$  with a unit cell length of  $3a/2 = 2.13 \text{ \AA}$ , which is half the unit cell length of a zigzag nanotube.

The subband dispersion relations are given by

$$E_q(k) = \pm \left| 1 + 4\cos\left(\frac{3ak}{2}\right)\cos\left(\frac{q\pi}{N}\right) + 4\cos^2\left(\frac{q\pi}{N}\right) \right|^{1/2} \quad (6)$$

Therefore, when  $N = 3k$ , there are two subbands with zero bandgap the tube is metallic. In the rest of the paper we distinguish between metallic or *crossing* subbands ( $q = N/3$  and  $2N/3$ ) and semiconducting or *non crossing* subbands.

The contacts are assumed to be reflectionless reservoirs maintained at equilibrium, i.e. they have well defined chemical potentials, equal to that of the metal leads:  $V_S$  in the source and  $V_D$  in the drain. Further, the nanotube and metal are assumed to have the same workfunction. The contact self-energies  $\Sigma_{c,q}^{R,<,>} = \Sigma_{S,q}^{R,<,>} + \Sigma_{D,q}^{R,<,>}$  due to the source contact are found [24] using the surface Green's function  $g_q^S$  of a semi-infinite nanotube, which is the solution of the following system of equations:

$$\begin{aligned} (a_1 - t_2^2 g_{2,q}^S) g_{1,q}^S &= 1 \\ (a_2 - t_1^2 g_{1,q}^S) g_{2,q}^S &= 1, \end{aligned} \quad (7)$$

where the indices 1 and 2 stand for the two sites of the unit cell and  $a_{1,2} = E - U_o - V_S$ . The Green's function

for the drain are solved for in a similar way, by making the following substitutions:  $t_{1,2}^S \rightarrow t_{2,1}^D$ ,  $g_{1,2,q}^S \rightarrow g_{1,2,q}^D$ .

For each subband  $q$  we solve a system of transport equations [24]:

$$(E - H^q - V - \Sigma_{c,q}^R(E))G^{R,q} = I \quad (8)$$

$$(E - H^q - V - \Sigma_{c,q}^R(E))G^{<,>,q} = \Sigma_{c,q}^{<,>}(E)G^{A,q} \quad (9)$$

Electron charge and current density  $n_i$  and  $J_i$  at each node  $i$  are found from the following equations:

$$n_i = -2i \sum_q \int_{-3t_o - eV_D}^{-eV_S + 10kT} G_{i,i}^{<,q}(E) \frac{dE}{2\pi} \quad (10)$$

$$J_i = \frac{4e}{\hbar} \sum_q \int_{-eV_D - 10kT}^{-eV_S + 10kT} G_{i,i+1}^{<,q}(E) t_{i+1,i}^q \frac{dE}{2\pi}, \quad (11)$$

where we used the fact that the band bottom at equilibrium is at  $-3t_o$ . To integrate the electron charge over energy, we employed a conventional approach developed in DFT ([21], [22], [23]) and described below. The technique drastically reduces the computational requirements as the whole band can be integrated with 200 energy grid points with error of  $10^{-6}$  of charge. The integral (10) is divided into equilibrium  $[-3t_o - eV_D; -eV_D - 10kT]$  and non-equilibrium parts  $[-eV_D - 10kT, -eV_S + 10kT]$ . In the equilibrium part of the energy spectrum, the current is zero and one can apply the fluctuation-dissipation theorem  $G^{<}(E) = -2if(E)\Im m[G^{R}(E)]$ , where Fermi factor  $f(E) = 1$  at these energies.  $G^R$  is analytical in the upper plain of complex energies which allows one to transform the integration of  $G^{<}$  over the real axis in the equilibrium part of energy spectrum to the integration of  $G^R$  over a complex contour  $C$  starting at  $-3t_o - eV_D$  and ending at  $-eV_D - 10kT$ . The non equilibrium part is integrated over the real axis from  $-eV_D - 10kT$  to  $-eV_S + 10kT$ :

$$n_i = -\frac{2}{\pi} \sum_q \oint_C \Im m[G_{i,i}^{R,q}(E)dE] - \frac{i}{\pi} \sum_q \int_{-eV_D - 10kT}^{-eV_S + 10kT} G_{i,i}^{<,q}(E)dE \quad (12)$$

In this work, corresponding to ballistic transport, we neglect electron-phonon scattering. The electron mean free path (mfp) is proportional to the matrix element squared and thus inversely proportional to the chirality index. Ref. [12] reported  $\lambda_o^{el} \approx 1.6 \mu m$  and  $\lambda_o^{in} \approx 10 \text{ nm}$  for a tube with a diameter of 1.8 nm, corresponding to a (24,0) nanotube. This allows us to assume that large diameter nanotubes of moderate lengths, e.g.  $\sim 100 \text{ nm}$  (240,0) nanotube, will remain nearly ballistic even at high bias. The ballistic transport is also an adequate approximation at low bias for all diameter nanotubes due to the absence of strong inelastic phonon emission.

We model the electrostatics of the nanotube as a system of point charges between the two contacts located at

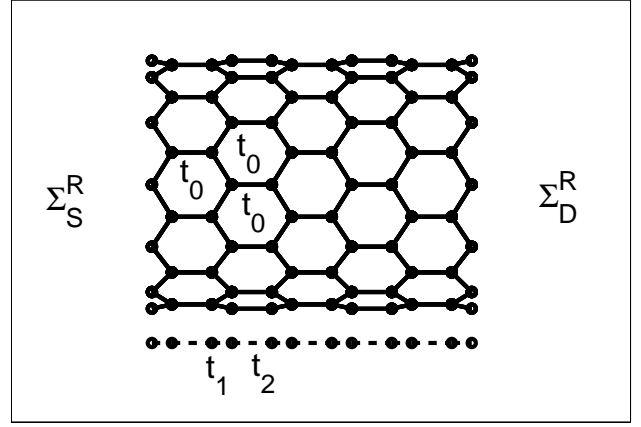


Fig. 1. Zigzag carbon nanotube and the corresponding 1D chain. The hopping parameter between nearest neighbors in the nanotube is  $t_o$ . The 1-D chain has two sites per unit cell with on-site potential  $U_o$  and hopping parameters  $t_1 = 2t_o \cos(\frac{\alpha}{2})$  and  $t_2 = t_o$

$y = y_S = 0$  and  $y = y_D = L$ . The "perfect contacts" are modeled as parallel semi-infinite three dimensional metal leads that are maintained at fixed source and drain potentials:  $V_S$  for  $y < y_S$  and  $V_D$  for  $y > y_D$ . So, while the self-energies due to contacts are identical to that of a semi-infinite nanotube, the role of electrostatics is included by image charges corresponding to a perfect metal. The electrostatic potential consists of a linear drop due to a uniform electric field created by the leads and the potential due to the charges on the tube and their images

$$V = -eV_S - e(V_D - V_S)(y - y_S)/(y_D - y_S) + \sum_j G(i,j)(n_j - N) \quad (13)$$

with the Green's function

$$G(i,j) = \frac{e}{4N\pi\epsilon_o} \sum_{n=-\infty}^{+\infty} \sum_l \left[ \frac{1}{\sqrt{(y_i - y_j + 2nL)^2 + \rho_{k,l}^2}} - \frac{1}{\sqrt{(y_i + y_j + 2nL)^2 + \rho_{k,l}^2}} \right]. \quad (14)$$

Here,  $\rho_{k,l}$  is the radial projection of the vector between atom  $k$  at ring  $i$  and atom  $l$  at ring  $j$ . The summation is performed over all atoms  $l$  at ring  $j$  for an arbitrary value of  $k$ . Maintaining the nanotube atoms buried in the metal at a fixed potential is close to reality because of the screening properties of 3D metals. Within a few atomic layers from the metal surface, the potential should have approached the bulk values. While the variation in potential in these few atomic layers of the 3D metal is not captured in our model, our conclusions on the nanotube electrostatics should not be significantly affected.

The calculations for one bias point involve iterations of (7-13) until convergence of the potential and charge distributions is achieved. The solution of (8-9) employs

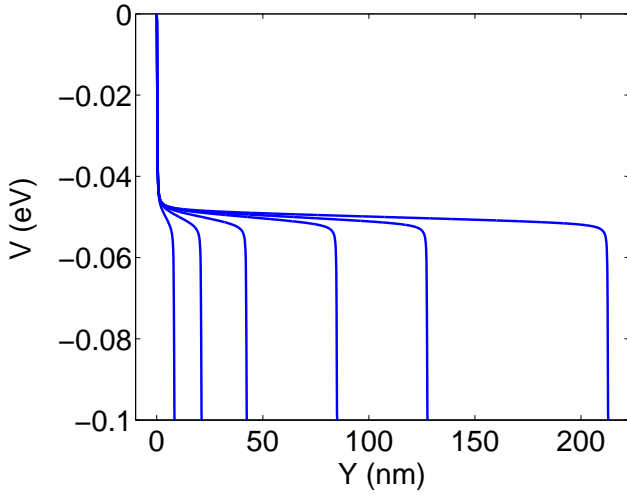


Fig. 2. Potential distribution versus position for (12,0) nanotubes of various lengths. The diameter of the (12,0) nanotube is 0.94 nm and the applied bias is 100 mV. Note the constant potential drop at the edges.

the recursive algorithm [24], which scales linearly with the number of nodes. The contour integral in (12) is taken using Gaussian quadratures.

### III. RESULTS

#### A. Electrostatics

At low biases (100 mV), electron-phonon scattering does not play a significant role in determining the potential distribution for wires of moderate length (less than few hundreds of nanometer). The potential distribution for (12,0) nanotubes of lengths varying from 21.3 to 213 nm are shown in Fig. 2. The edges of the nanotube near the contact rapidly screen the applied bias / electric field. The screening is due to the free electron density provided by the crossing subbands. The potential drop is divided unequally between different parts of the nanotube, with 90% of the applied bias dropping within 1 nm from the edges for both lengths considered here. Note, that in the ballistic regime, resistance of the nanotube does not depend on tube length, which results in the drop at the edges being constant for all tube lengths.

While the total density of states (DOS) per unit length of metallic nanotubes is independent of diameter, the DOS per subband and free charge carried by the crossing subbands are inversely proportional to the diameter. As a result, we find that the screening in metallic nanotubes degrades with diameter. The potential drop for nanotubes with diameters of 0.94 nm [(12,0) nanotube], 2.82 nm [(36,0)] and 4.7 nm [(60,0)] are shown in Fig. 3. Clearly, screening is poorer in the larger diameter nanotube. In fact, while the potential drops by 45 mV in a distance of 1 nm from the edge for the (12,0) nanotube, the potential drops for (36,0) and (60,0) are only 37 mV and 31 mV

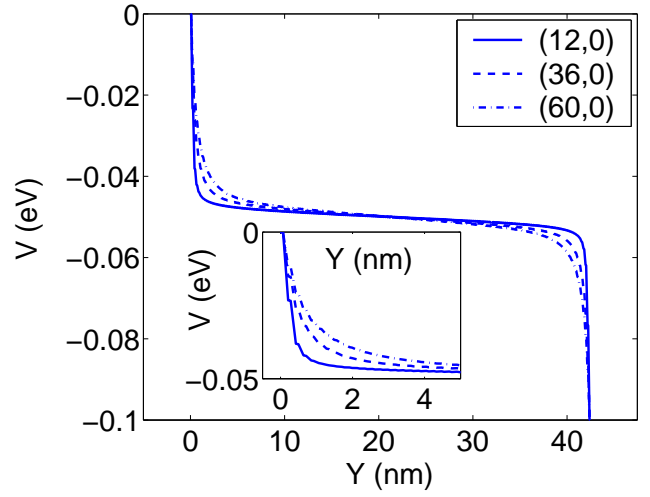


Fig. 3. Potential versus position for (12,0), (36,0) and (60,0) nanotubes, with diameters 0.94, 2.82 and 4.7 nm. The screening for the large diameter nanotubes is poorer. The inset magnifies the potential close to the edge of the nanotube. The applied bias is 100 mV.

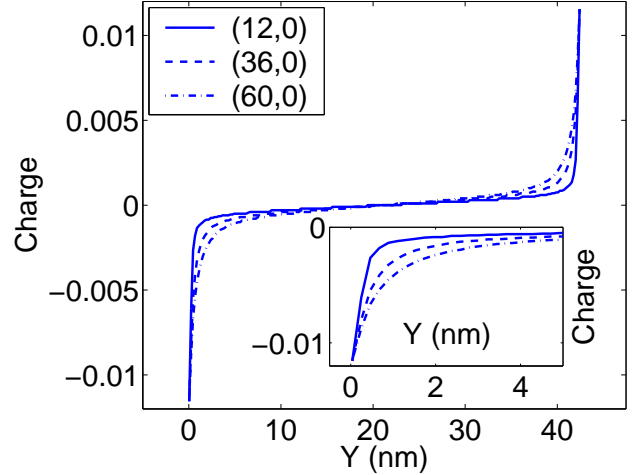


Fig. 4. Charge density versus position for (12,0), (36,0) and (60,0) nanotubes. The inset magnifies the charge distribution close to the edge of the nanotube. The applied bias is 100 mV.

respectively. The inset of Fig. 3 shows a substantially larger electric field away from the edges of the large diameter nanotube. Another difference between large and small diameter nanotubes is due to the different geometry contained in the electrostatic Green's function (14). Higher number of atoms per ring in larger diameter tubes slightly offsets the deterioration of screening due lower density of states.

Fig. 4 shows the self-consistent charge profiles, corresponding to the potential in Fig. 3. The interplay between the competing factors of different density of states and electrostatic Green's function results in different charge profiles. In the larger diameter tubes more charge is

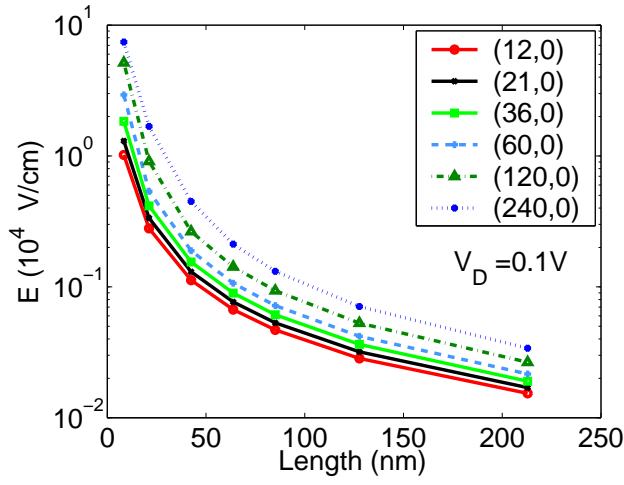


Fig. 5. This plot shows the electric field at the mid point versus nanotube length for various nanotube diameters at an applied bias of 100 mV. The electric field decreases approximately as  $1/L^{1.25-1.75}$ .

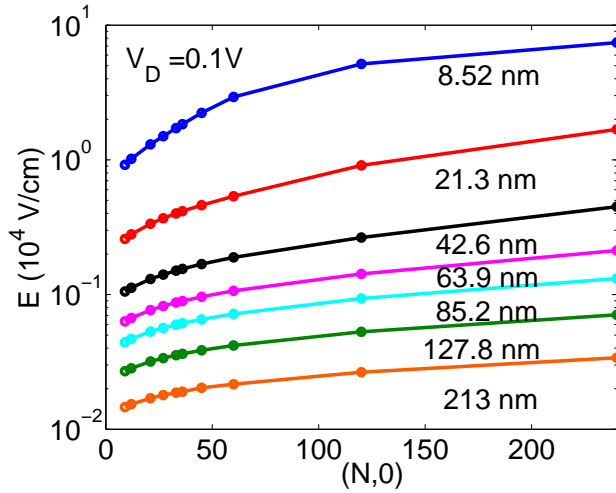


Fig. 6. The electric field at the mid point versus nanotube chirality index for various lengths at an applied bias of 100 mV. The electric field increases approximately as  $N^{0.25-0.75}$ .

accumulated at the edges.

The electric field at the center of the nanotube as a function of length is shown in Fig. 5 for the tube with a diameter of 0.94 nm. We find that for all diameters, the electric field decreases more rapidly than  $\frac{1}{L}$ , where  $L$  is the length of the nanotube. The exact power law however depends on the diameter. If the computed electric field versus length is fit to  $\frac{1}{L^a}$ , the exponent  $a$  increases with increase in diameter. The value of  $a$  increases from 1.25 to 1.75 as the diameter increases from 0.94 to 18.85 nm. The dependence of the electric field on the chirality index of the tube is shown in Fig. 6. The electric field versus diameter ( $D = aN/\pi$ ) can be fit to  $D^b$ , where  $b$  is in the range of 0.25 and 0.75. The presence of non zero electric

field inside a conducting nanotube is not totally surprising: it is a consequence of a lower electron density of states in 1D.

### B. Transport

We now discuss the current-voltage characteristics as a function of bias for small and large diameter nanotubes of length 42.6 nm, in the ballistic limit. The ballistic current and differential conductance for the different diameters are shown in Fig.7 and Fig.8. For the moderate diameter nanotubes ( $N < 90$ ), only two crossing subbands contribute to transport. The current increases linearly with applied bias and the differential conductance is  $4e^2/h$ .

In large diameter nanotubes ( $N = 90, 120$  and  $240$ ), ballistic current shows super linear increase. The conductance of large diameter nanotubes starts increasing after a threshold bias. This increase occurs due to Zener tunneling contribution of the non crossing subbands: when the bias becomes larger than twice the bandgap of the lowest non crossing subband, electrons can tunnel from valence band states ( $E < -E_g^{non}/2 + V(y)$ ) in the source to the conduction band states ( $E > E_g^{non}/2 + V(y)$ ) in the middle of the tube (the channel) and also from valence band states in the channel to the conduction band states in the drain. The lowest non crossing subbands ( $q = N/3 \pm 1$ ) in (90,0), (120,0) and (240,0) have bandgaps  $E_g^{non} = 331, 249$  and  $125$  meV respectively and start to contribute to current at biases of twice these values. In the ballistic limit, the self-consistently calculated current of (240,0) nanotube at 1 V is  $310 \mu A$  and the differential conductance is almost  $13e^2/h$ , signifying that a large number of subbands are contributing to current. As the barrier width at energies corresponding to valence band edge in the source  $E_v^S$  and conduction band edge in the drain  $E_c^D$  decreases with bias, the transmission and Zener tunneling current increase. The density of states (DOS) in the lowest non crossing subband in (240,0) nanotube at a bias of 0.4 V is shown in Fig. 9. Note the increased DOS in the bandgap at energies  $E_v^S$  and  $E_c^D$ .

Another qualitative difference occurs at zero bias in (240,0) nanotube (Fig.8). The zero bias conductance of (240,0) nanotube is larger than  $4e^2/h$  because the non crossing subbands are partially filled and contribute to current: the first non crossing subband opens at an energy of  $2.4 kT$  from the band center. This contribution is a simple intraband transport, determined by the population of the conduction band in the source and the valence band in the drain, but rather insensitive to the details of the potential distribution. At slightly higher biases the non crossing subbands contribution to current saturates to a constant value and the contribution to differential conductance decreases to zero, while the total conductance decreases to  $4e^2/h$ .

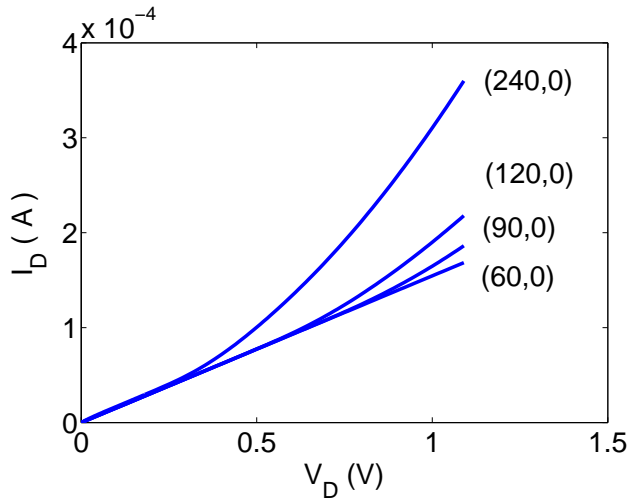


Fig. 7. The current-voltage characteristics of large diameter nanotubes in the ballistic limit. The current shows faster than linear increase with bias due to the contribution of non crossing subbands.

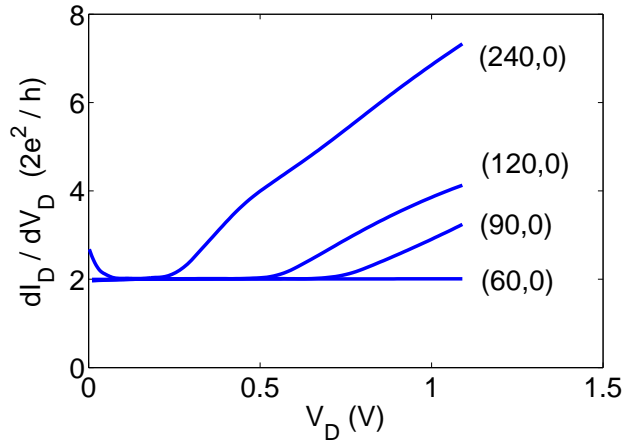


Fig. 8. The differential conductance as a function of bias in the ballistic case. Contribution of non crossing subbands in (240,0) nanotube leads to the non monotonic behavior of conductance. High bias increase corresponds to Zener tunneling and is determined by the bandgap of the lowest non crossing subband.

To elucidate the effect of non crossing subbands further, Fig.10 shows the evolution with bias of current versus electron energy in the lowest non crossing subband. At low biases there are two peaks in the current density corresponding to partially filled valence and conduction bands. The height of the peaks increases only slightly and then saturates at all higher biases. These peaks in the current density are responsible for the increased value of zero bias conductance. When bias is higher than twice the bandgap, two new peaks in the current density occur at  $E_v^S$  and  $E_c^D$ , corresponding to Zener tunneling at the source and drain respectively. The height of these peaks increases rapidly due to the exponential dependence on the barrier

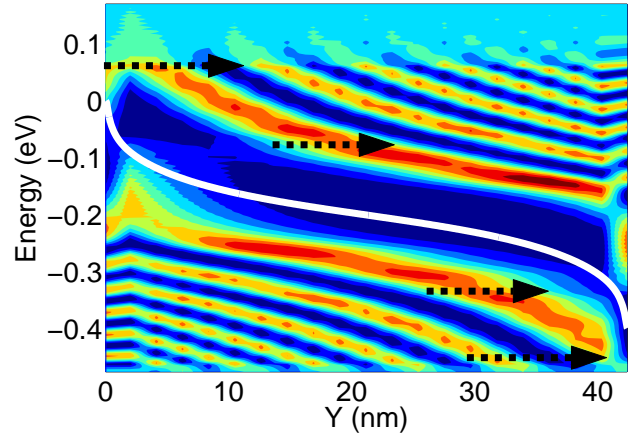


Fig. 9. Local density of states in the lowest non crossing subband of a (240,0) nanotube under a bias of 0.4 V as a function of position and energy. Brighter color shows higher DOS. Also shown is the potential profile. The arrows correspond to four contributions to a current due to the non crossing subband in Fig.10

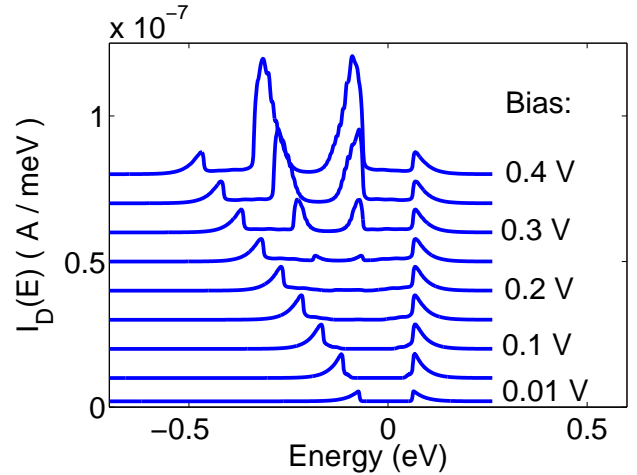


Fig. 10. A set of current density versus energy curves due to the lowest non crossing subband in a (240,0) nanotube under different biases. Two outermost peaks correspond to transport in the valence and conduction bands. Two inner peaks correspond to Zener tunneling between valence and conduction band states.

width.

The important consequence of the different origin of these four peaks is the temperature dependence of differential conductance. At low temperatures, the outermost peaks will vanish, reducing the value of conductance to  $4e^2/h$ . However, the height and shape of the inner peaks are insensitive to the temperature which implies the robustness of Zener tunneling.

In conclusion, we find that in the ballistic (low bias/large diameter) regime, applied bias drops mostly at the edges. However, the 1-dimensionality of the nanotube leads to

very slow ( $\sim 1/L^\alpha$ ) screening of the electric field as compared to a bulk crystal. In agreement with experimental measurements of Ref. [17], our calculations show larger electric field for larger diameter nanotubes. The conductance of large diameter nanotubes shows non monotonic bias dependence: at low and high bias the conductance is higher than  $4e^2/h$  due to the contribution of non crossing subbands.

We are grateful to Dr. Hatem Mehrez for his help with the complex contour integration of DOS.

#### REFERENCES

- [1] B. Q. Wei, R. Vajtai and P. M. Ajayan, *Appl. Phys. Lett.* **79**, 1172-1174 (2001)
- [2] F. Kreupl, A. P. Graham, G. S. Duesberg, W. Steinhogel, M. Liebau, E. Unger and W. Honlein, *Microelectron. Eng.* **64**, 399-408 (2002)
- [3] Q. Ngo, D. Petranovic, S. Krishnan, A. M. Cassell, Q. Ye, J. Li, M. Meyyappan and C. Y. Yang, *IEEE Trans. Nanotech.* **3**, 311 (2004)
- [4] P. J. de Pablo, E. Graugnard, B. Walsh, R. P. Andres, S. Datta and R. Reifenberger, *Appl. Phys. Lett.* **74**, 323 (1999)
- [5] S. Frank, P. Poncharal, Z. L. Wang and W. A. de Heer, *Science* **280**, 1744 (1998)
- [6] P. Poncharal, S. Frank, Z. L. Wang and W. A. de Heer, *Eur. Phys. J. D* **9**, 77 (1999)
- [7] J. Nygard, D. H. Cobden, M. Bockrath, P. L. McEuen and P. E. Lindelof, *Appl. Phys. A* **69**, 297-304 (1999)
- [8] J. Kong, E. Yenilmez, T. W. Tombler, W. Kim, H. Dai, R. B. Laughlin, L. Liu, C. S. Jayanthi, and S. Y. Wu, *Phys. Rev. Lett.* **87**, 106801 (2001)
- [9] Z. Yao, C. L. Kane and C. Dekker, *Phys. Rev. Lett.*, **84**, 2941 (2000)
- [10] P. G. Collins, M. Hersam, M. Arnold, R. Martel and Ph. Avouris, nanotubes, *Phys. Rev. Lett.* **86**, 3128-3131 (2001)
- [11] P. J. de Pablo, C. Gomez-Navarro, J. Colchero, P. A. Serena, J. Gomez-Herrero and A. M. Baro, *Phys. Rev. Lett.*, **88**, 36804 (2002)
- [12] J. Park, S. Rosenblatt, Y. Yaish, V. Sazonova, H. Ustunel, S. Braig, T. A. Arias, P. W. Brouwer and P. L. McEuen, *Nano Lett.* **4**, 517 (2004)
- [13] G. Pennington and N. Goldsman, electrons in semiconducting carbon nanotubes *Phys. Rev. B* **68**, 045426 (2003)
- [14] P. Poncharal, C. Berger, Y. Yi, Z. L. Wang and W. A. de Heer, *J. Phys. Chem. B* **106**, 12104 (2002)
- [15] Y. X. Liang, Q. H. Li and T. H. Wang, *Appl. Phys. Lett.* **84**, 3379-3381 (2004)
- [16] M. P. Anantram, *Phys. Rev. B* **62**, 4837 (2000)
- [17] A. Bachtold, M. S. Fuhrer, S. Plyasunov, M. Forero, E. H. Anderson, A. Zettl and P. L. McEuen, *Phys. Rev. Lett.*, **84**, 6082 (2000)
- [18] F. Leonard and J. Tersoff, *Phys. Rev. Lett.*, **83**, 5174 (1999)
- [19] S.J. Tans, M. Devoret, H. Dai, A. Thess, R.E. Smalley, L.J. Geerligs, and C. Dekker, *Nature*, v. 386, p. 474 (1997)
- [20] M. P. Anantram, *Appl. Phys. Lett.*, v. 78, p. 2055 (2001)
- [21] A. R. Williams, P. J. Feibelman, N. D. Lang, *Phys. Rev. B* **26**, 5433 (1982)
- [22] J. Taylor, H. Guo, J. Wang, molecular electronic devices *Phys. Rev. B* **63**, 245407 (2001)
- [23] M. Brandbyge, J.-L. Mozos, P. Ordejón, J. Taylor, K. Stokbro, *Phys. Rev. B* **65**, 165401 (2002)
- [24] A. Svizhenko, M. P. Anantram, T.R. Govindan, R. Venugopal, *J. Appl. Phys.*, **91**, 2343 (2002)